Chapter 3

Non-linear finite element analysis

In this chapter, the Grisham algorithm is further verified. The Grisham algorithm results for the *example problem in the previous chapter* are now compared with the results of a complete non-linear finite element analysis.

3.1 Overview

Global load control methods (e.g. the arc-length control method proposed by Riks and Wempner [11, 12]) are suitable for global buckling and post-buckling analysis. However, they are not ideal when the buckling is localized (when there is a local transfer of strain energy from one part of the model to neighbouring parts). Alternatives are to analyze the problem dynamically, or to introduce an artificial damping factor. In the dynamic case, the strain energy released during local buckling is transformed into kinetic energy; in the damping case the strain energy is dissipated. To solve a quasi-static problem dynamically is expensive, however.

Hence, the modified Riks algorithm, combined with damping, is selected as an analysis option in the ABAQUS® environment. The modified Riks method is used where the load magnitudes are controlled by a single scalar parameter. The load is considered unknown and the algorithm solves for loads and displacements simultaneously. An arc length along the equilibrium path is used as an indication of the progress of the solution and can be used to specify the termination of the analysis. To account for instability in the non-linear static problem, volume-proportional damping is added to the model. This provides viscous forces that are large enough to prevent instantaneous collapse, but small enough not to affect the results while the problem is stable and is a computationally efficient approach for the analysis of localized buckling.

The damping factor is determined in such a way that the extrapolated dissipated energy is a small fraction of the extrapolated strain energy. The damping factor is dependent on the mesh size and material behavior.

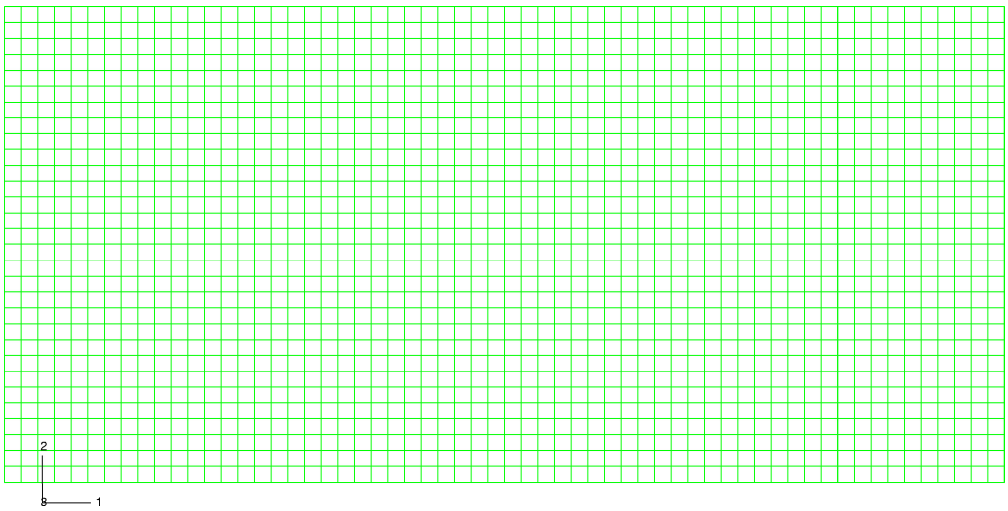

Figure 3.1: Non-linear finite element mesh

3.2 The finite element model

Again, the flanges and uprights are modelled using second order beam elements with the appropriate cross-section. The eccentricity of the single uprights (angles on one side of the web only) is taken into account. The web is modelled using isoparametric, second order, thin shell elements. Figure 3.1 shows the mesh used in the non-linear analysis, which is much more dense than the mesh used in the linear analysis for Grisham's algorithm. In the non-linear analysis 10×30 elements were used for the web of each panel as opposed to the 3×3 in the linear analysis. A distributed, vertical shear load is applied at the one end. The flanges as well as upright number 7 are constrained not to deform out of the plane.

3.3 Web results

The onset of shear buckling occurs after 13 load increments at an applied shear load of 1 552 N, resulting in a nominal web shear stress of $\tau_{cr} = 3.370$ MPa, which is slightly higher than the values predicted by the Grisham algorithm ($\tau_{cr} = 2.624$ MPa), the Wagner method ($\tau_{cr} = 2.358$ MPa) and the NACA approach ($\tau_{cr} = 2.551$ MPa). The three above methods, however, assume all four edges to be simply supported when calculating the buckling coefficients. This is conservative since the flanges and uprights are not completely flexible in torsion. The non-linear finite element method takes the torsional stiffness of the flanges and uprights into account and therefore gives a more accurate, higher critical stress value. A less conservative analytical estimate by Fehrenbach [7] gives a value of $\tau_{cr} = 3.195$ MPa for this problem. The

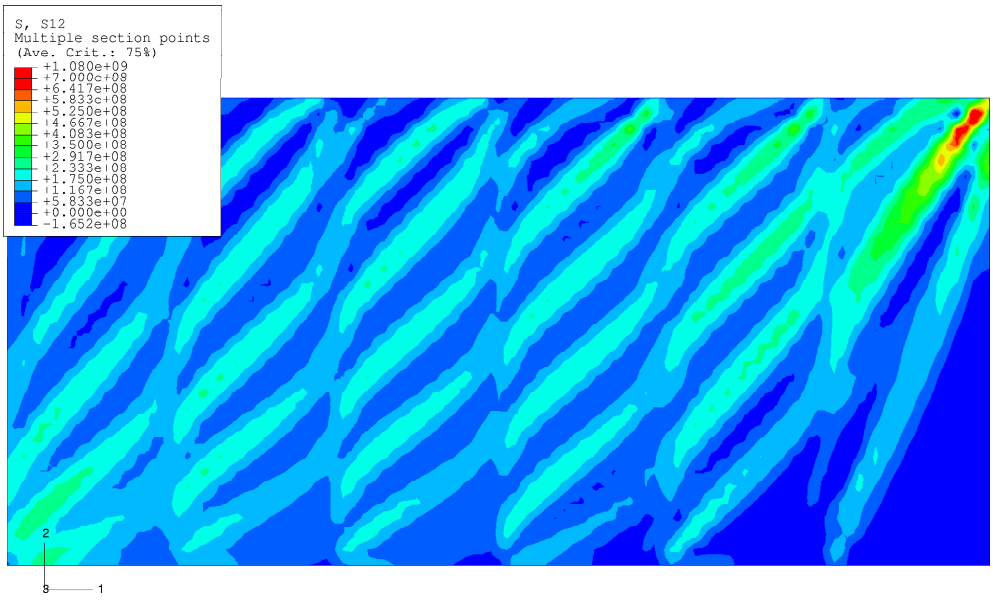

Figure 3.2: Shear stress (τ_{xy}) at the end of the analysis

analysis takes 102 load increments to reach the fully applied load of 60 048 N. The applied load of 60 048 N is almost 39 times more than the initial buckling load of 1 552 N, showing that the structure can hold a load orders of magnitude larger than the initial buckling load.

The stress results are shown in Figures 3.2 to 3.4. Figure 3.2 shows the shear stresses while Figures 3.3 and 3.4 shows the maximum and minimum principal stresses respectively. The effects of the folds in the web are clear as are the angles of the folds relative to the beam axis.

3.4 Upright results

Table 3.1 shows the non-linear finite element results in the uprights compared with the Grisham algorithm results (see Figure 2.8 for the location of the section points). The average stress values compare well for section points 5 and 9. At section point 1 the average stress results of the non-linear finite element analysis are slightly lower than the Grisham algorithm results, varying by up to 50 %. This shows that the out of plane bending effects due to the upright eccentricity is less evident in the non-linear finite element analysis. Except for upright number 2, the maximum stress values of the non-linear finite element analysis are higher than the Grisham algorithm results at all section points for all other uprights. The values vary from 0.8 % to 34 %.

The non-linear finite element upright stress result plots are shown in Figures 3.5 to 3.7. The upright stresses are negative at section points 5 and 9, indicating that the upright is in

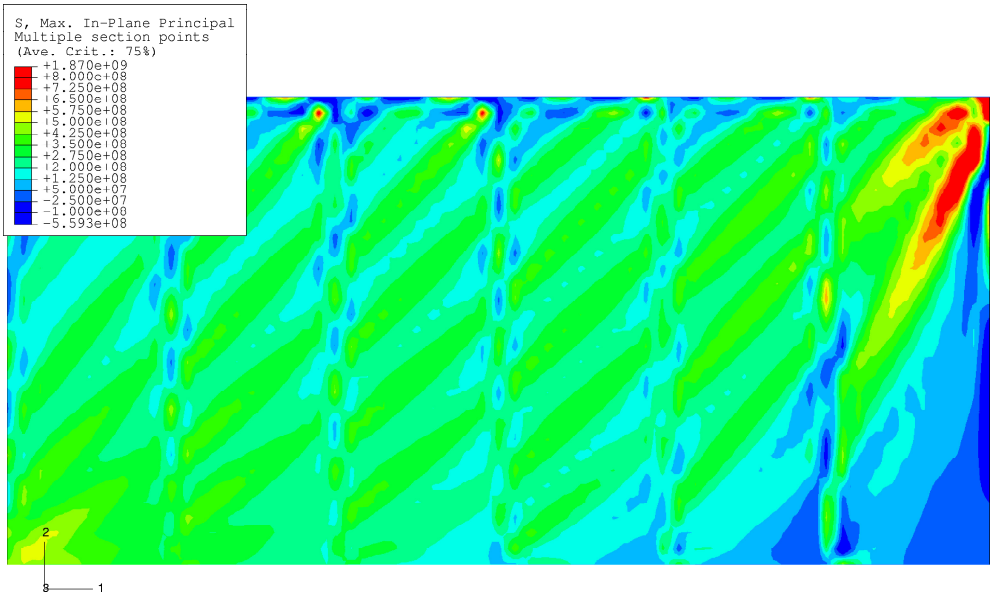

Figure 3.3: Maximum principal stress (σ_1) at the end of the analysis

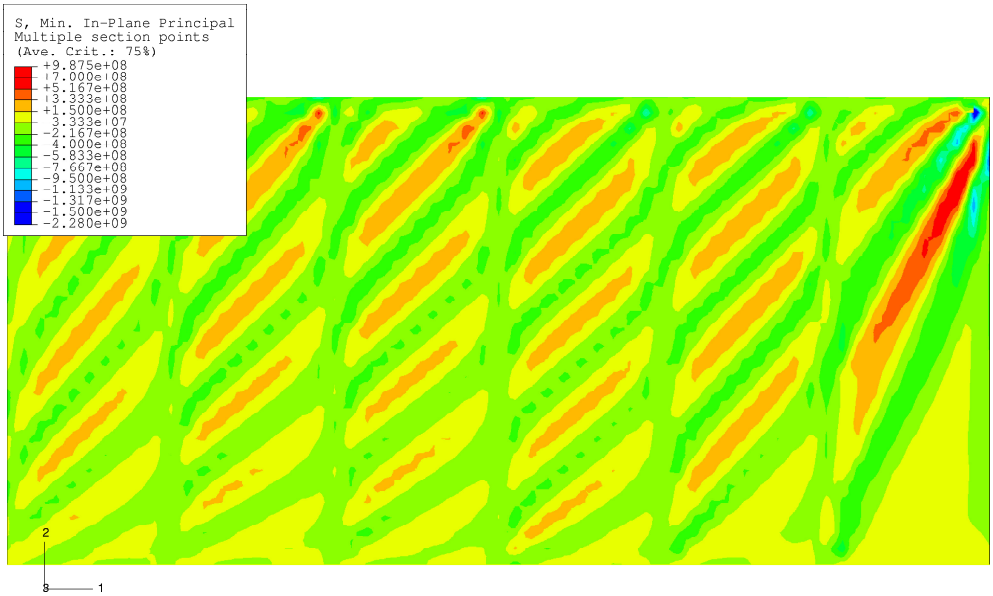

Figure 3.4: Minimum principal stress (σ_2) at the end of the analysis

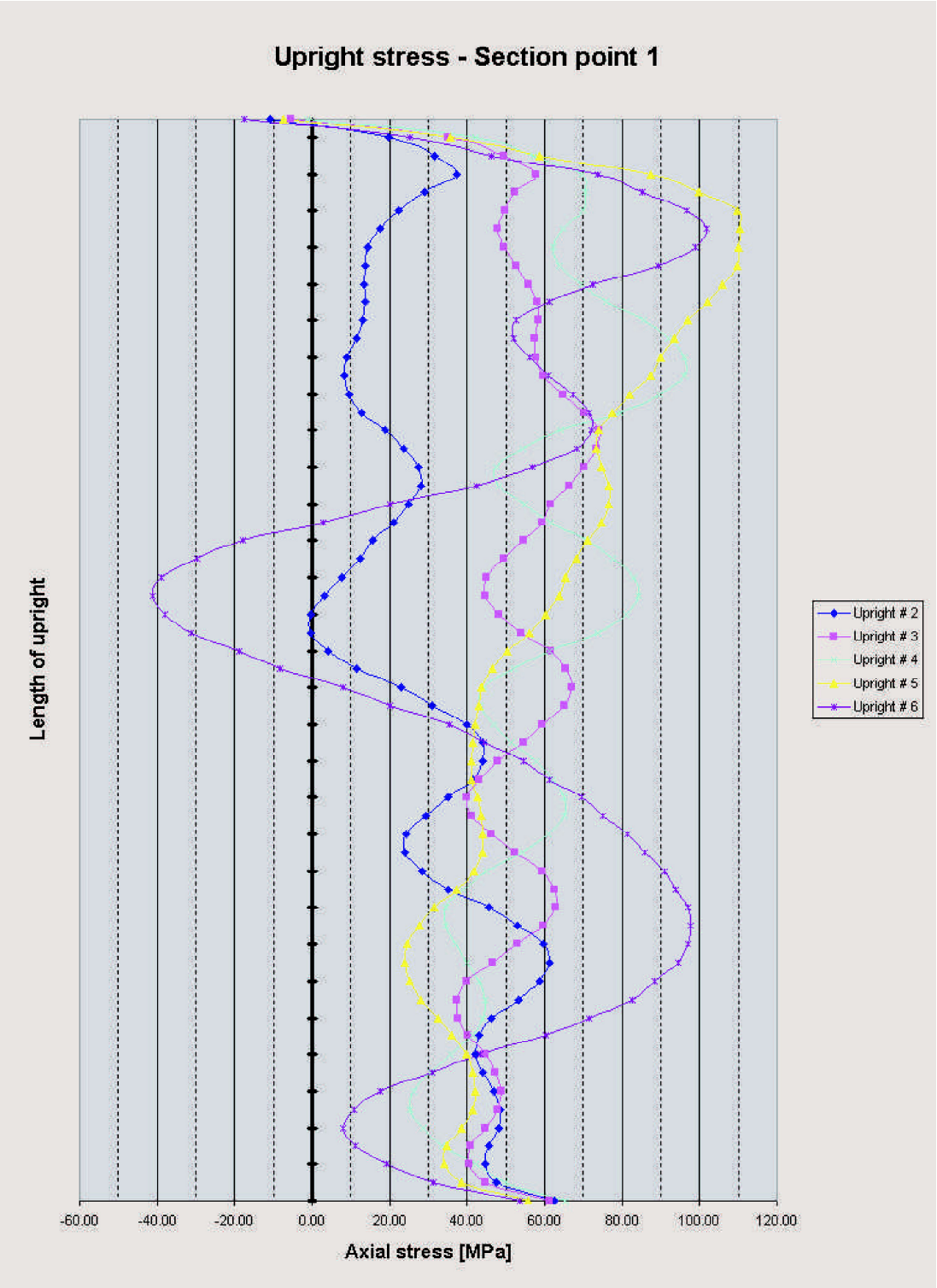

Figure 3.5: Stresses along the uprights at section point 1

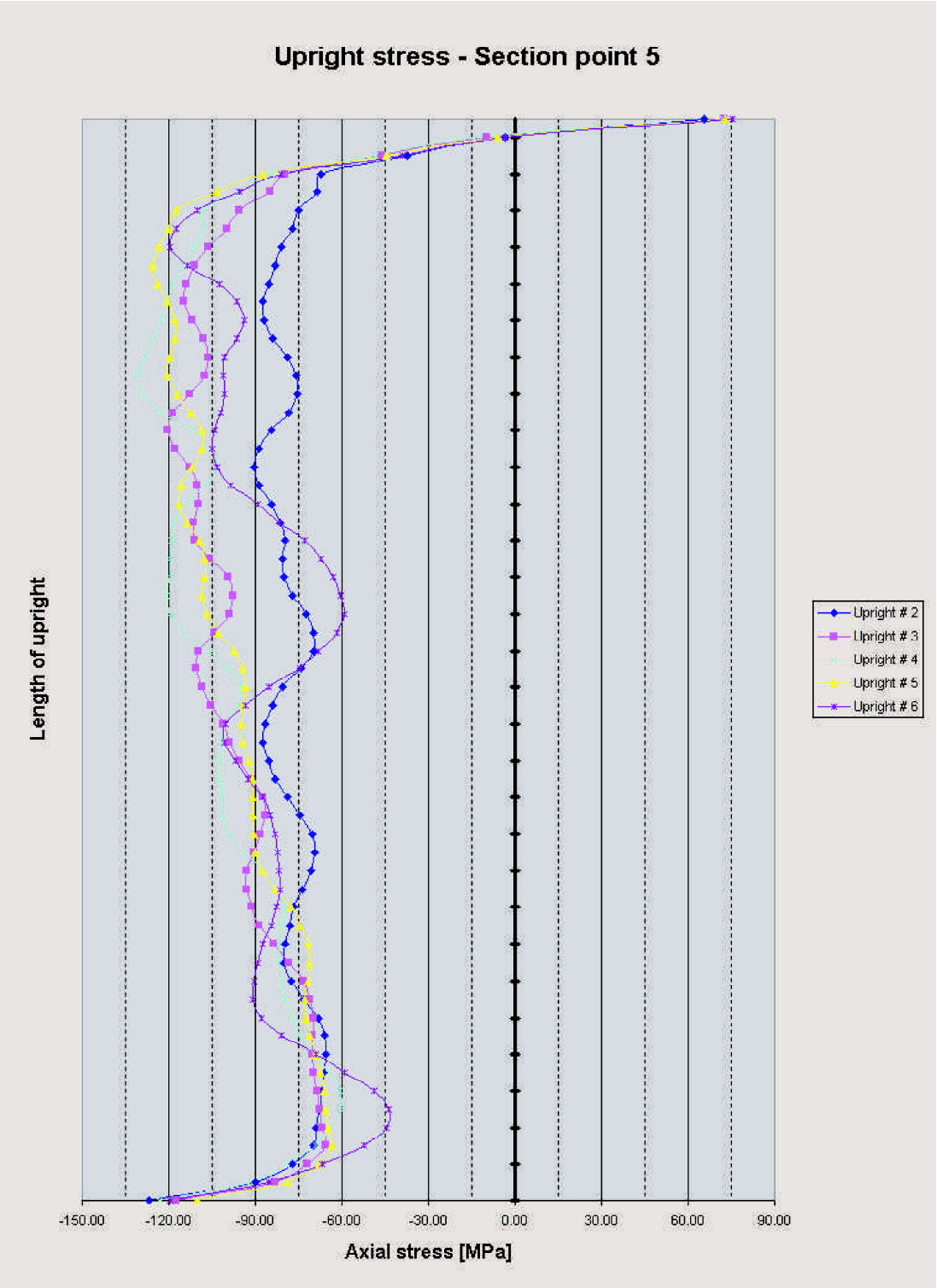

Figure 3.6: Stresses along the uprights at section point 5

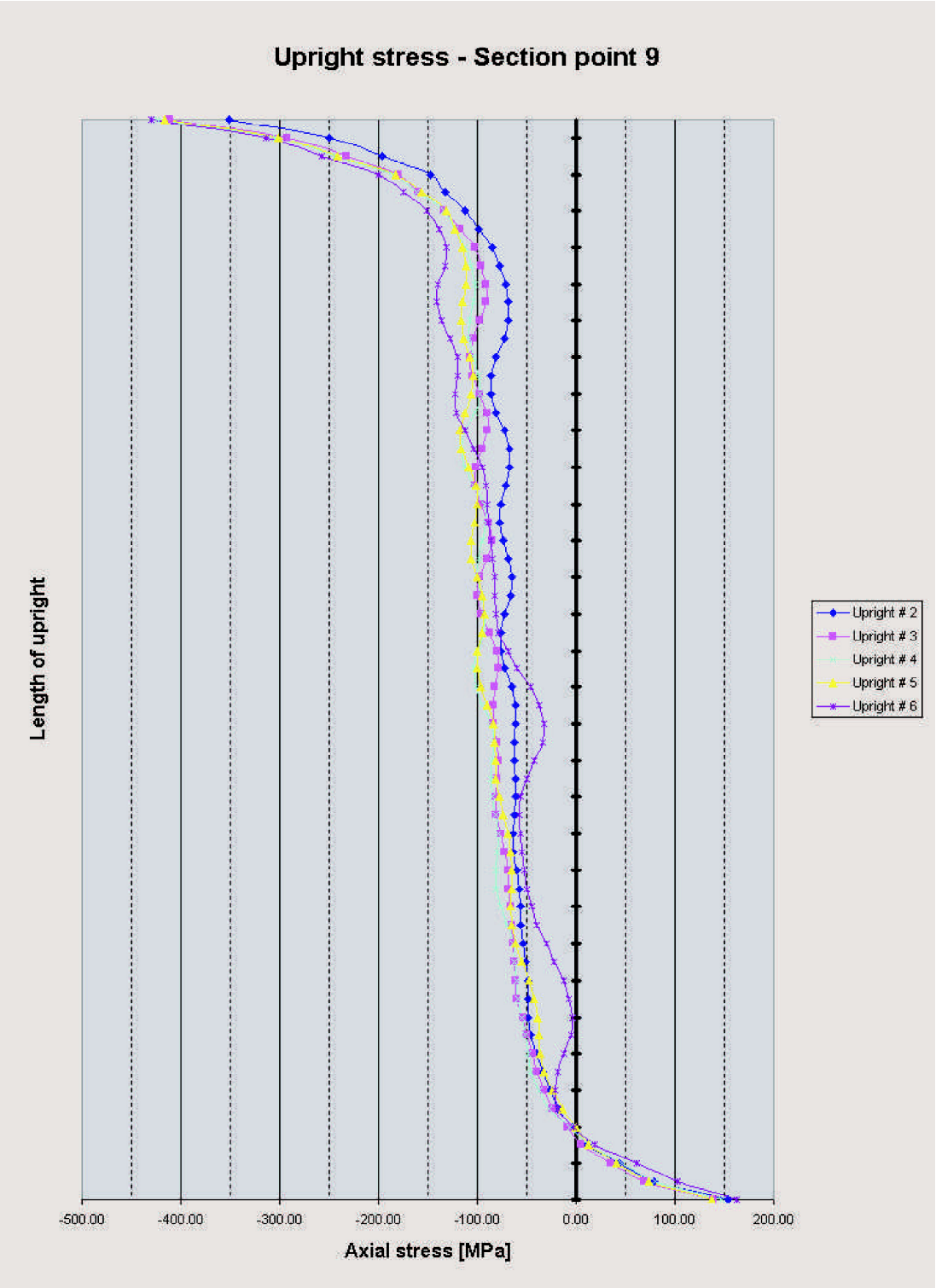

Figure 3.7: Stresses along the uprights at section point 9

	Six panel cantilever beam example - Bruhn [8]				
	Upright 2	Upright 3	Upright 4	Upright 5	Upright 6
$\overline{\sigma}_u$ (sp 1) - Grisham	51.2	73.2	77.1	72.9	67.3
$\overline{\sigma}_u$ (sp 1) - NL FEM	26.83	54.54	59.07	59.54	48.42
$\overline{\sigma}_u$ (sp 5) - Grisham	-74.2	-100.6	-102.6	-95.5	-85.8
$\overline{\sigma}_u$ (sp 5) - NL FEM	-78.29	-98.01	-102.25	-98.01	-87.39
$\overline{\sigma}_u$ (sp 9) - Grisham	-68.6	-98.8	-102.2	-95.5	-64.7
$\overline{\sigma}_u$ (sp 9) - NL FEM	-65.31	-81.77	-88.03	-85.74	-71.32
$\sigma_{u_{max}}$ (sp 1) - Grisham	69.3	85.7	84.2	88.1	67.7
$\sigma_{u_{max}}$ (sp 1) - NL FEM	61.35	73.98	96.09	110.36	101.65
$\sigma_{u_{max}}$ (sp 5) - Grisham	-101.2	-119.6	-115.7	-104.0	-89.6
$\sigma_{u_{max}}$ (sp 5) - NL FEM	-90.44	-120.64	-130.83	-125.69	-119.48
$\sigma_{u_{max}}$ (sp 9) - Grisham	-71.4	-109.4	-118.7	-118.7	-92.8
$\sigma_{u_{max}}$ (sp 9) - NL FEM	-99.21	-117.81	-122.24	-122.97	-141.72

Table 3.1: Upright stress results: non-linear finite element analysis

compression in the area attached to the web while the stresses at section point 1 are positive. This is due to bending of the upright out of the plane, as a result of the eccentric loading. Very high stresses occur at the two ends of the uprights at their attachment points to the flanges. This is especially evident from the graphs of section points 5 and 9. These peak stresses were ignored when calculating the average stress values and also when selecting the maximum stress value in each upright. The top and bottom three elements in each upright are ignored. These very high stresses are not realistic. In the finite element model, the attachment point of the uprights to the flanges are at a single node, resulting in very rigid joints with zero relative rotation of the joined elements. In practice, the uprights are riveted to the vertical leg of the flange by two or more rivets that introduce a measure of flexibility, thereby reducing the stresses at the extremities of the upright.

At high loading ratios ($\frac{\tau_{xy}}{\tau_{cr}} \gg 1$) the parabolic distribution in the upright flattens out according to the NACA. This is also evident from the results of the non-linear finite element analysis. The sinusoidal shape of the plots are due to the wrinkling effects of the web on the upright. To compare the stress distribution in the uprights for the two approaches, plots of each upright are made for the non-linear finite element model and the Grisham algorithm, at each section point. The comparative results for the five uprights, at each section point, are shown in Figures 3.8 to 3.22. The results of the two plots for section points 5 and 9 (adjacent to the web), compare very well. The results for section point 1 (the upright leg perpendicular to the web and loaded eccentrically) are more erratic although the average values still compare well.

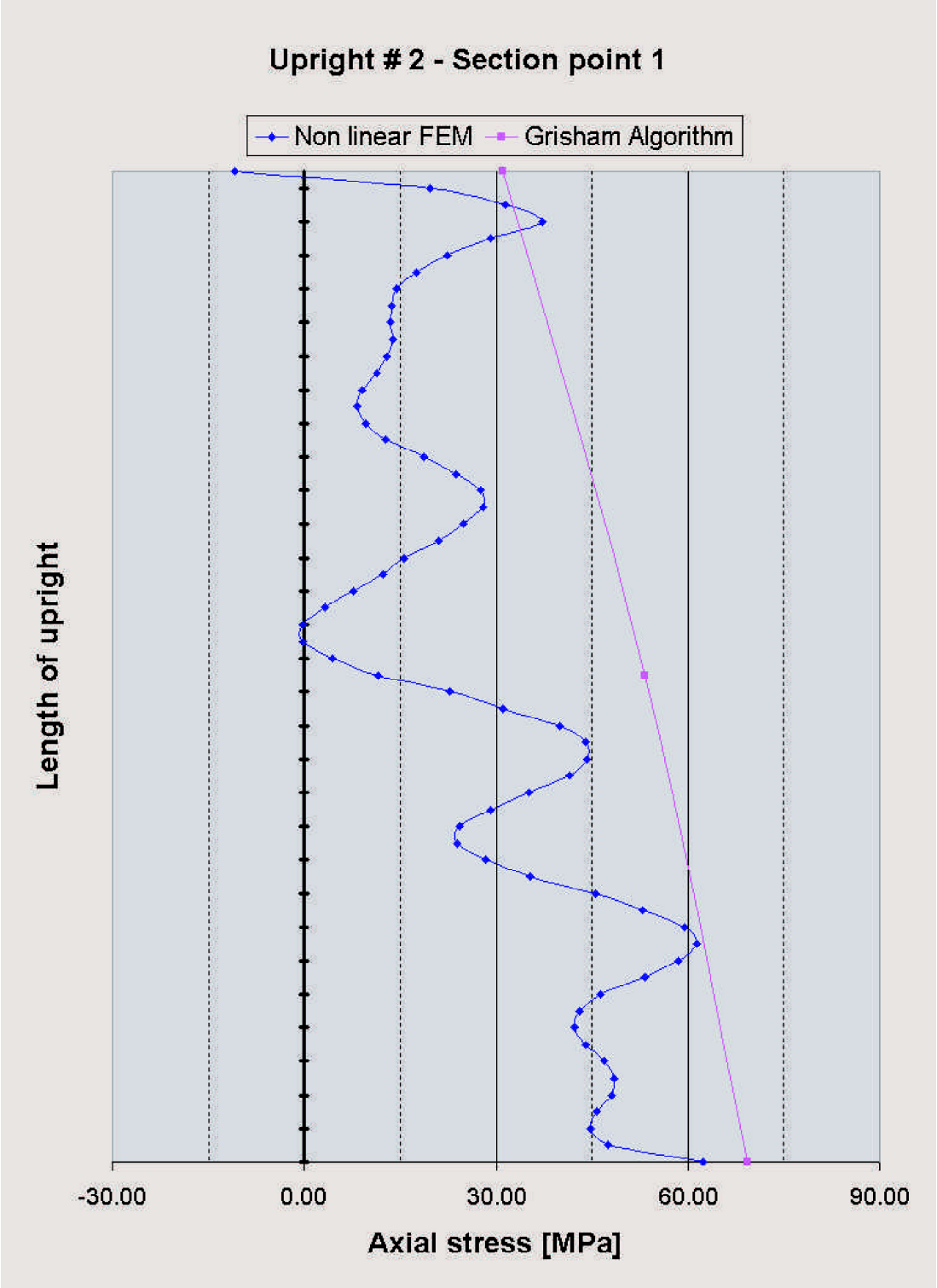

Figure 3.8: Comparative stress values in upright 2 at section point 1

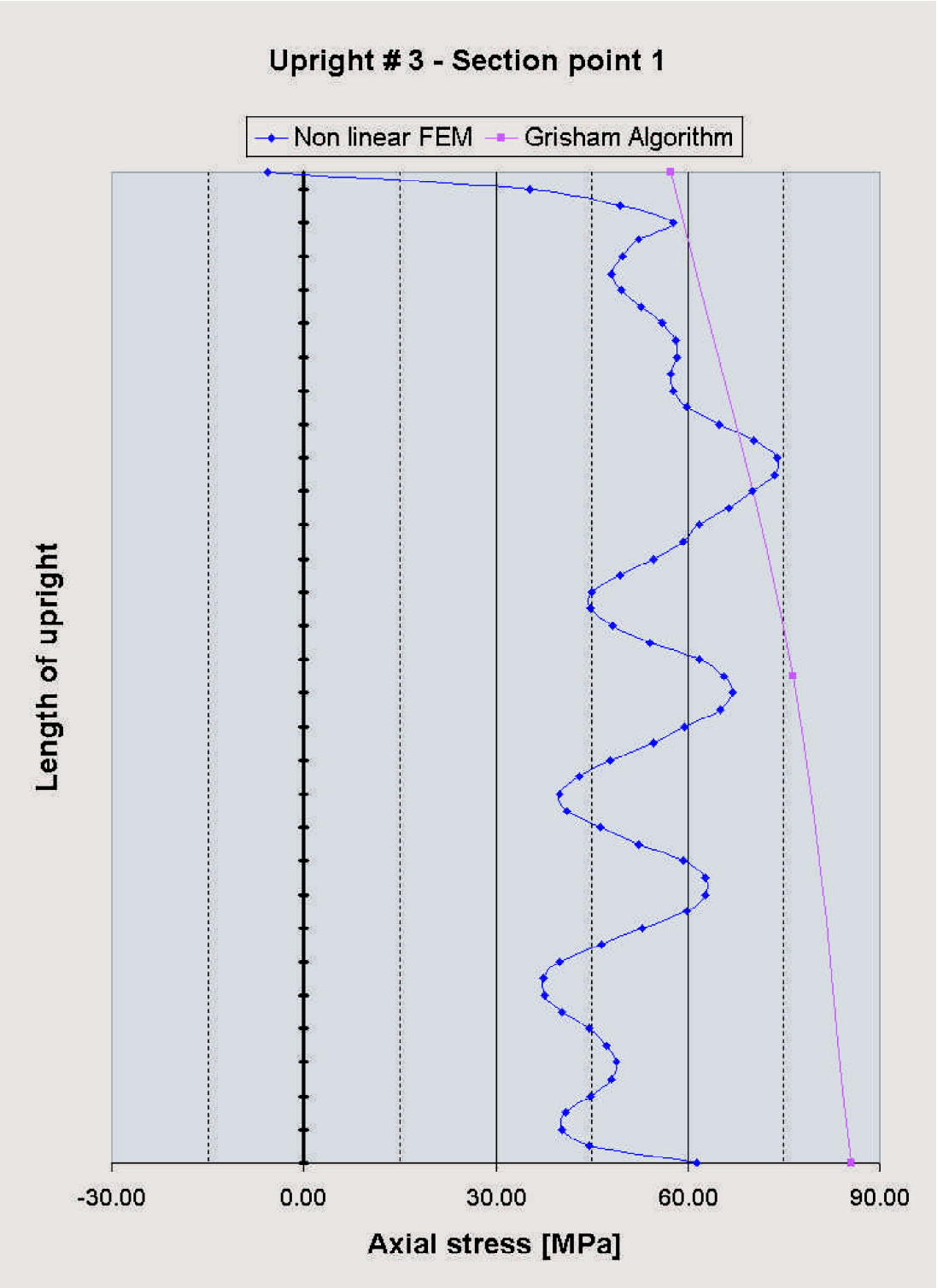

Figure 3.9: Comparative stress values in upright 3 at section point 1

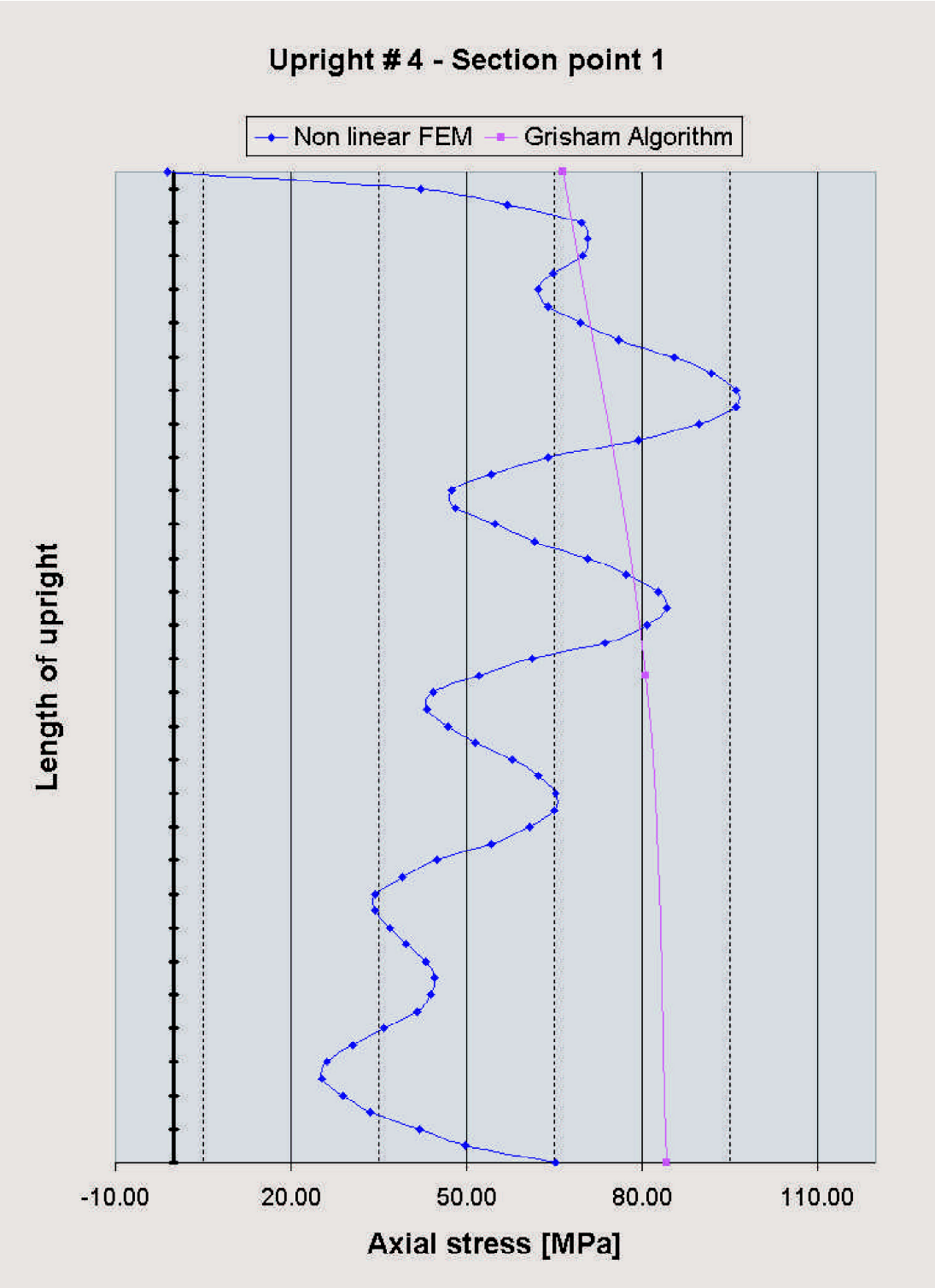

Figure 3.10: Comparative stress values in upright 4 at section point 1

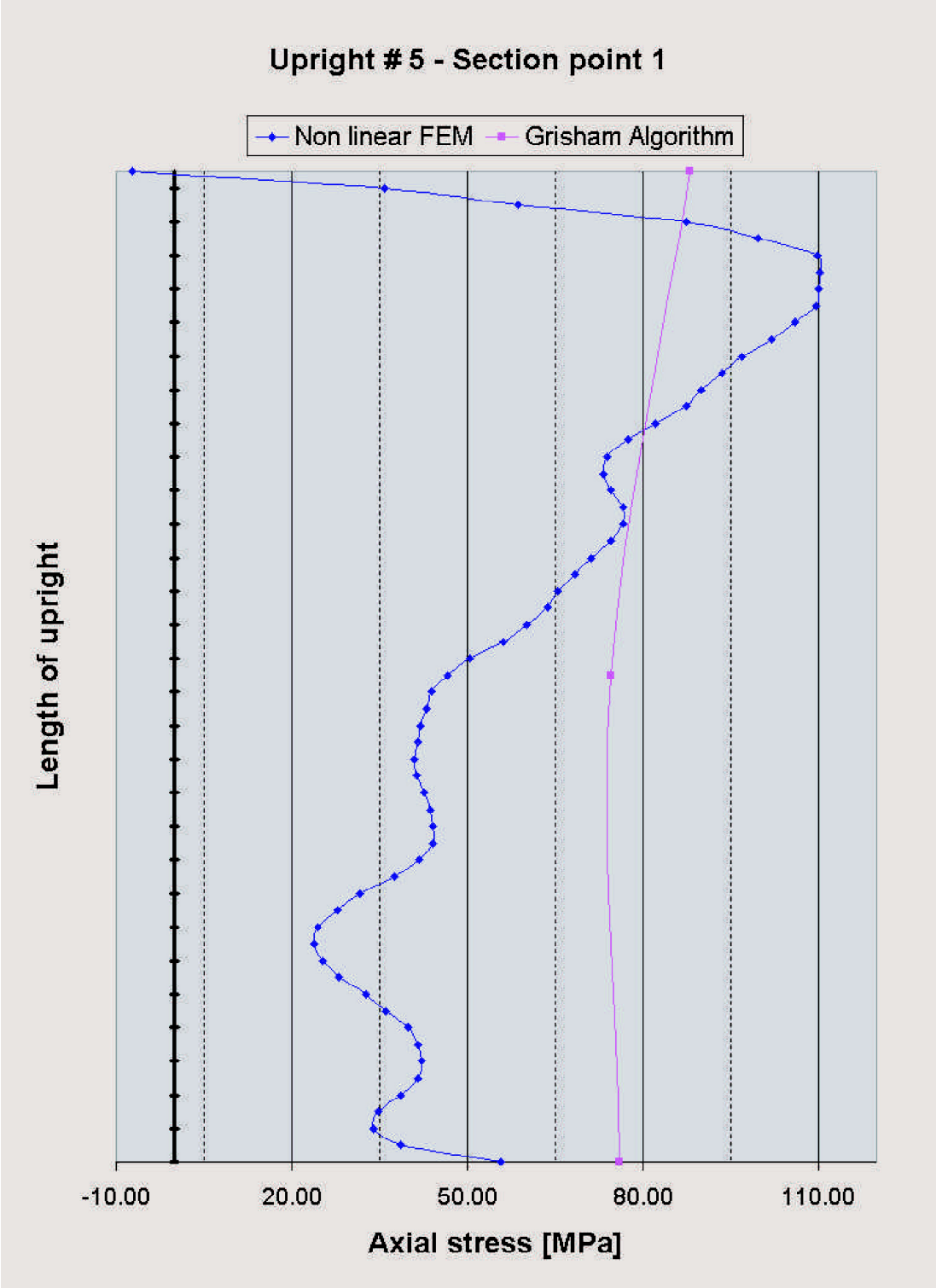

Figure 3.11: Comparative stress values in upright 5 at section point 1

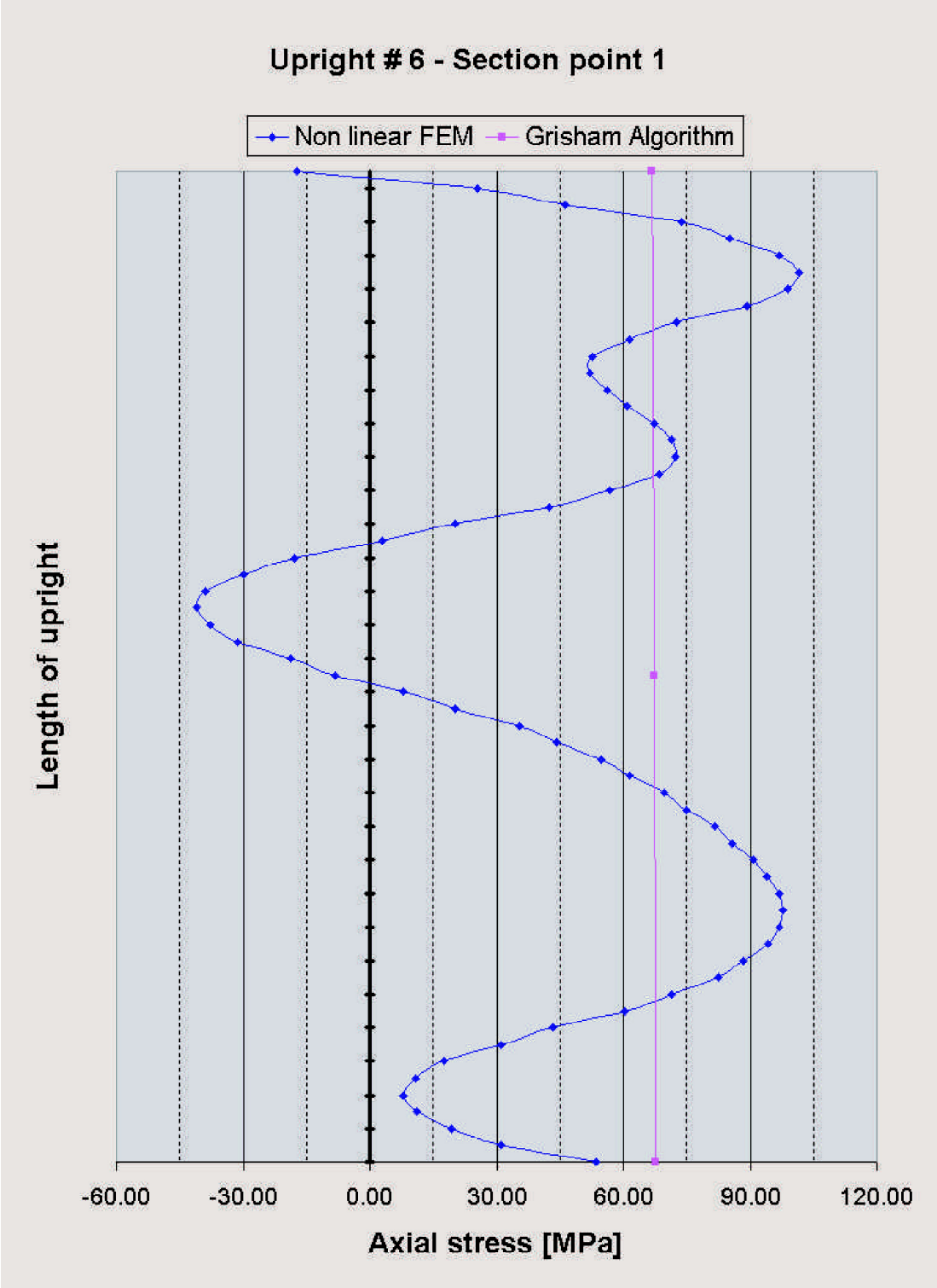

Figure 3.12: Comparative stress values in upright 6 at section point 1

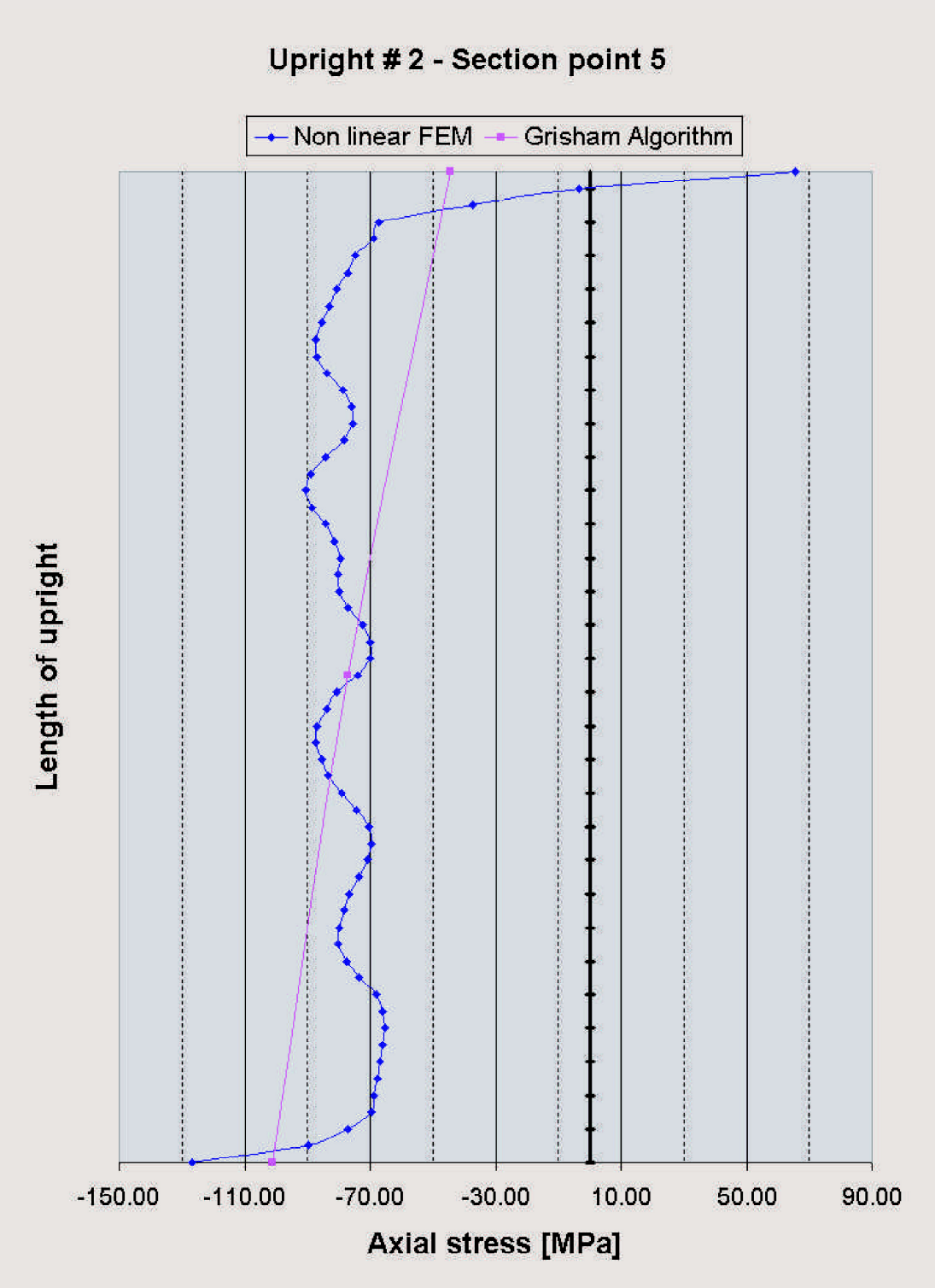

Figure 3.13: Comparative stress values in upright 2 at section point 5

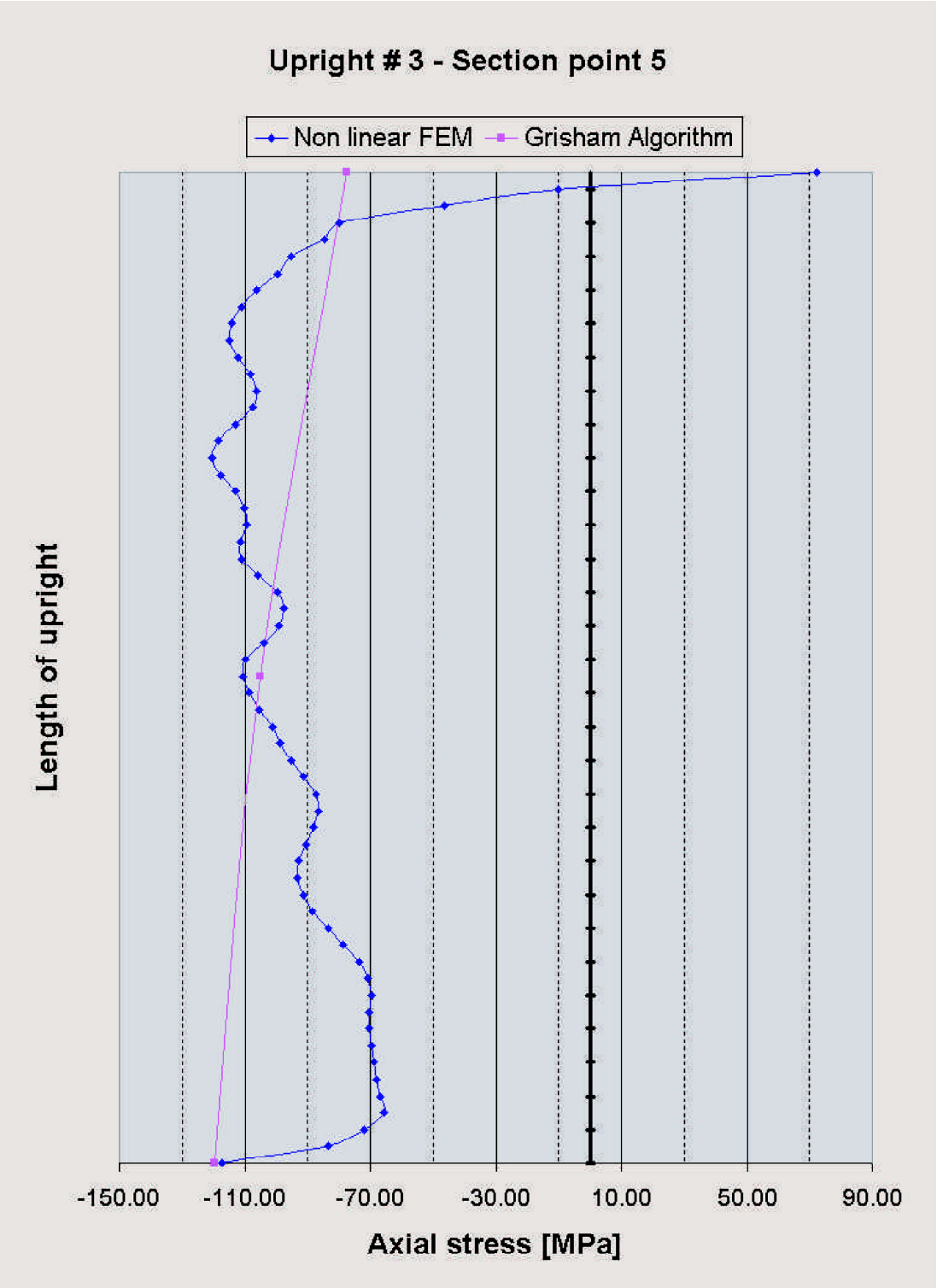

Figure 3.14: Comparative stress values in upright 3 at section point 5

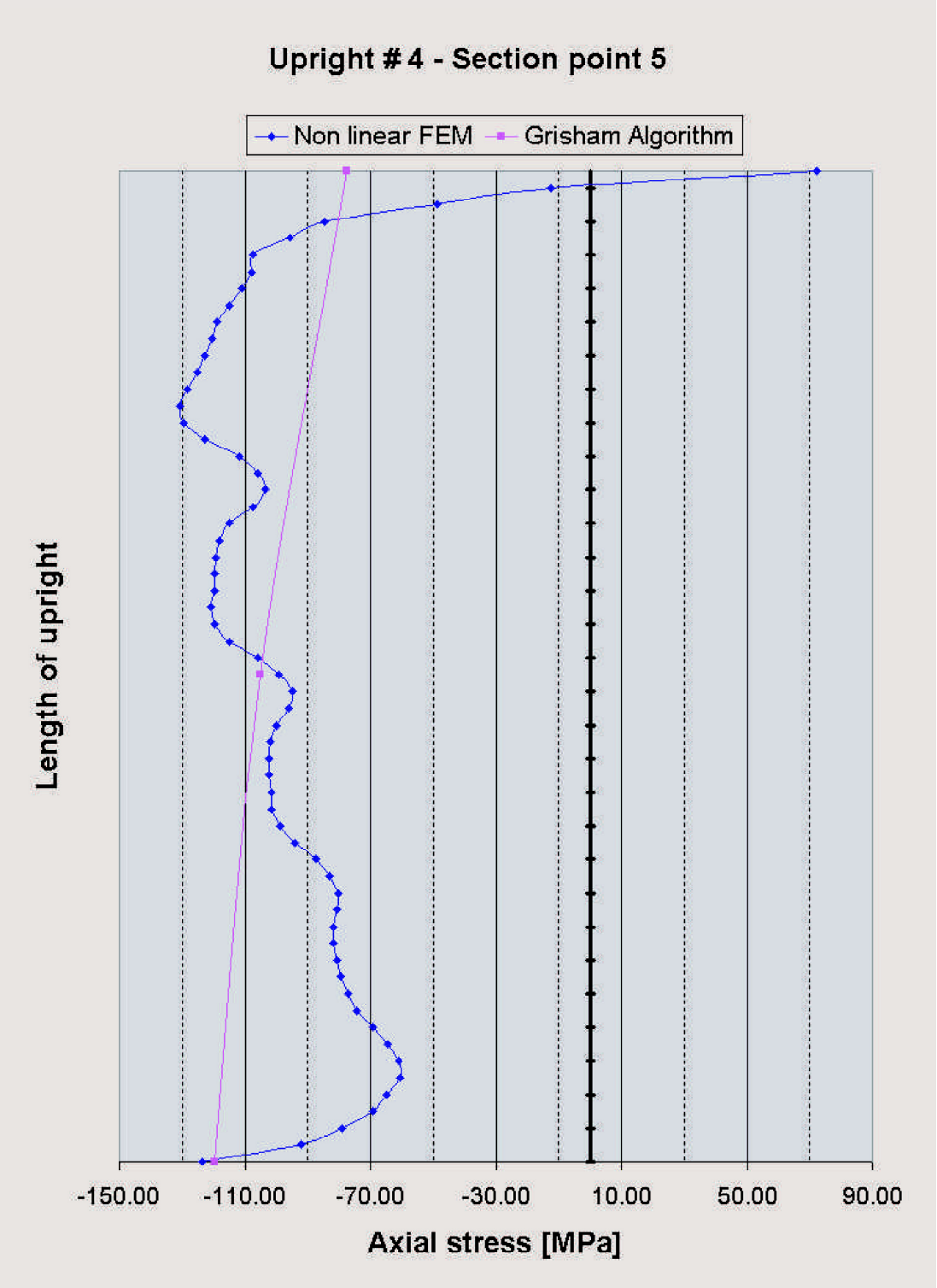

Figure 3.15: Comparative stress values in upright 4 at section point 5

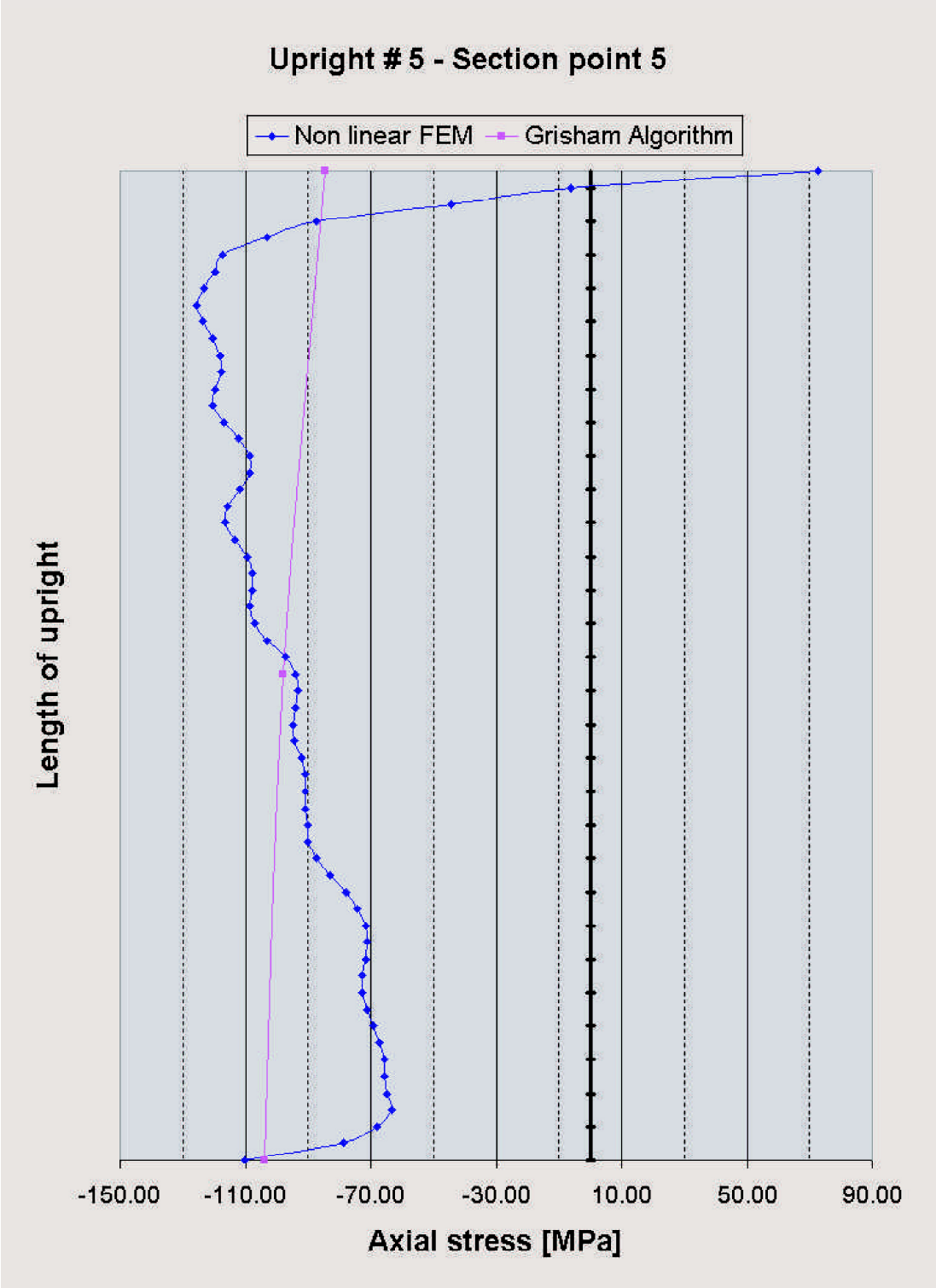

Figure 3.16: Comparative stress values in upright 5 at section point 5

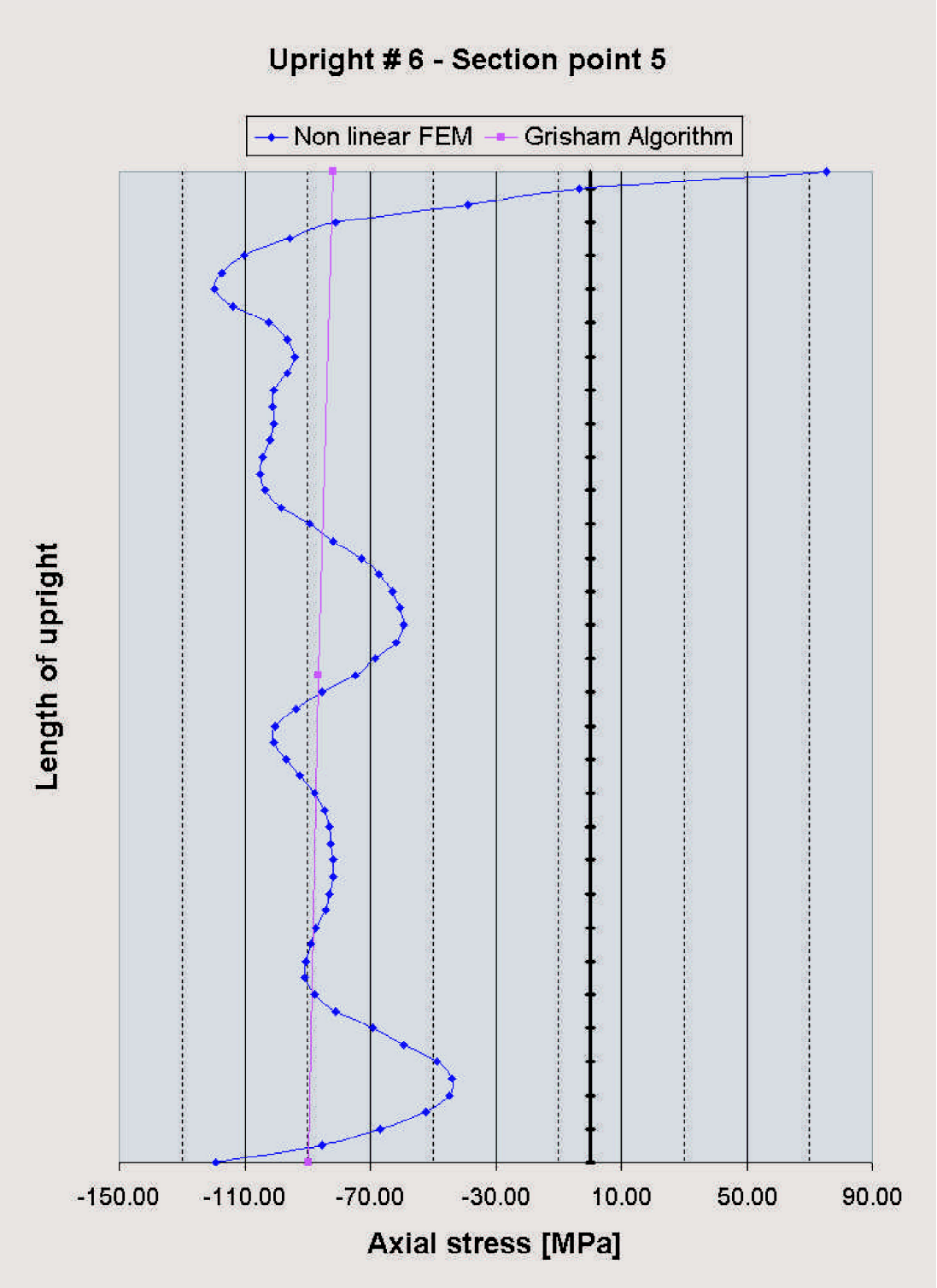

Figure 3.17: Comparative stress values in upright 6 at section point 5

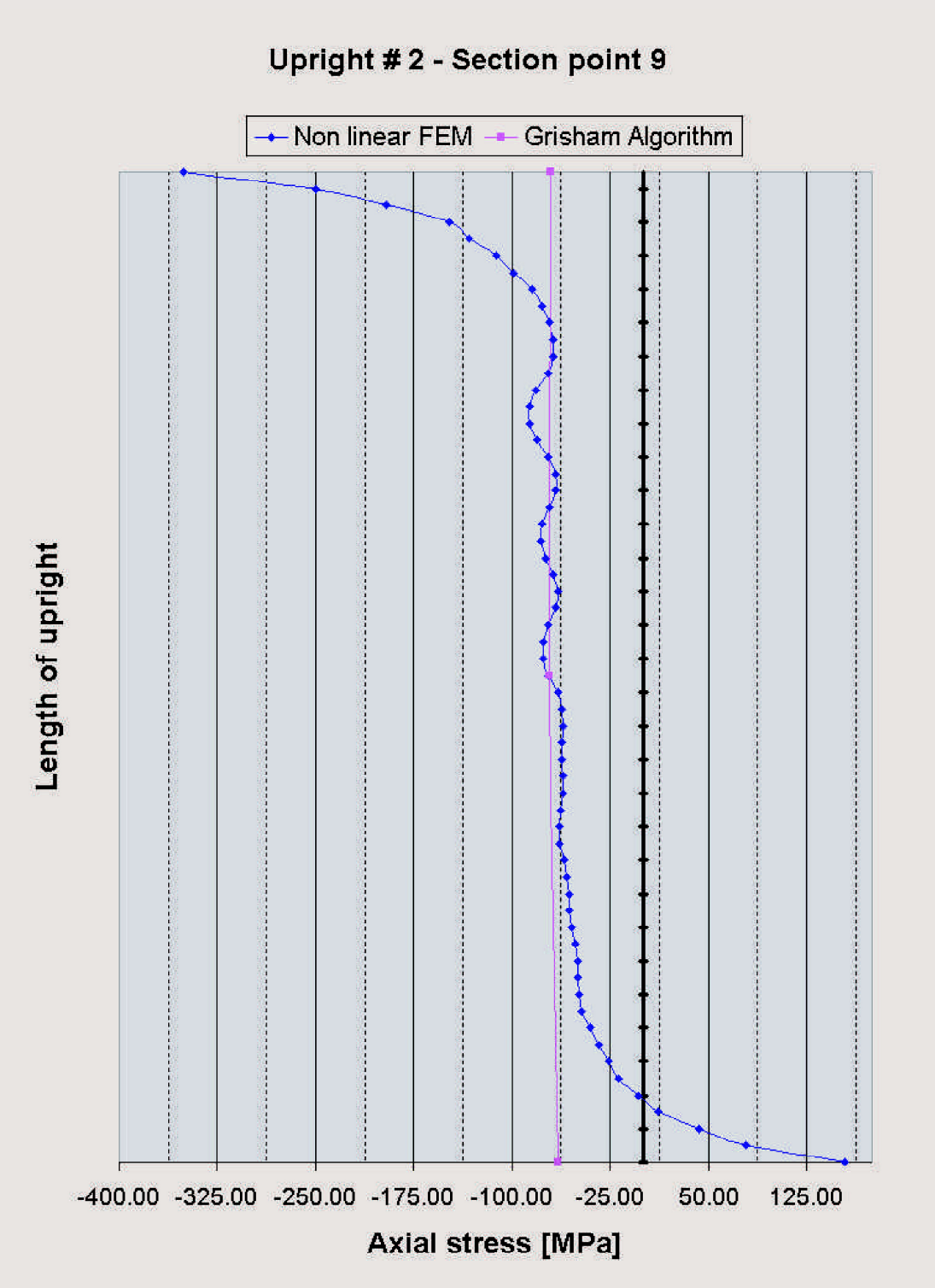

Figure 3.18: Comparative stress values in upright 2 at section point 9

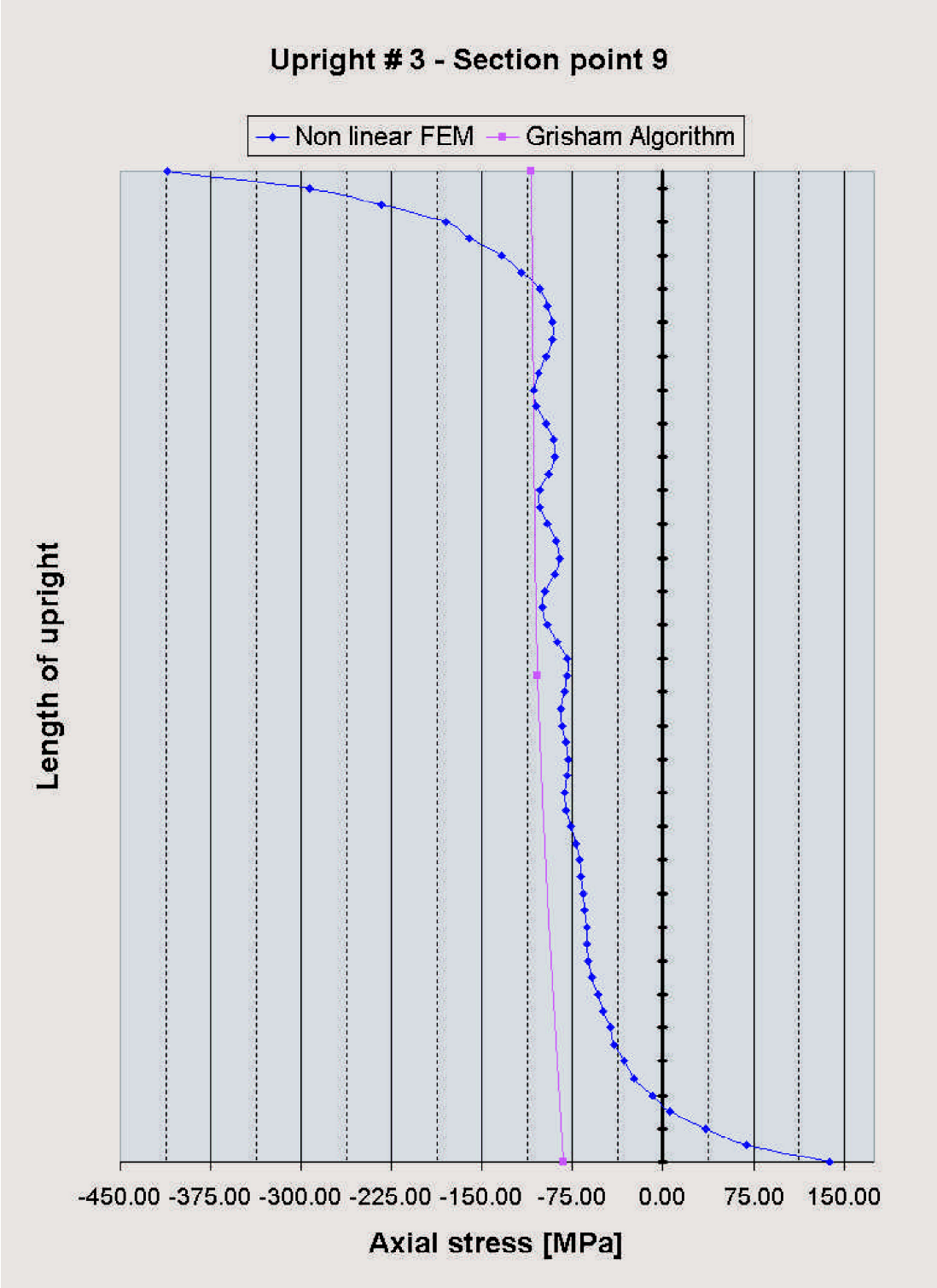

Figure 3.19: Comparative stress values in upright 3 at section point 9

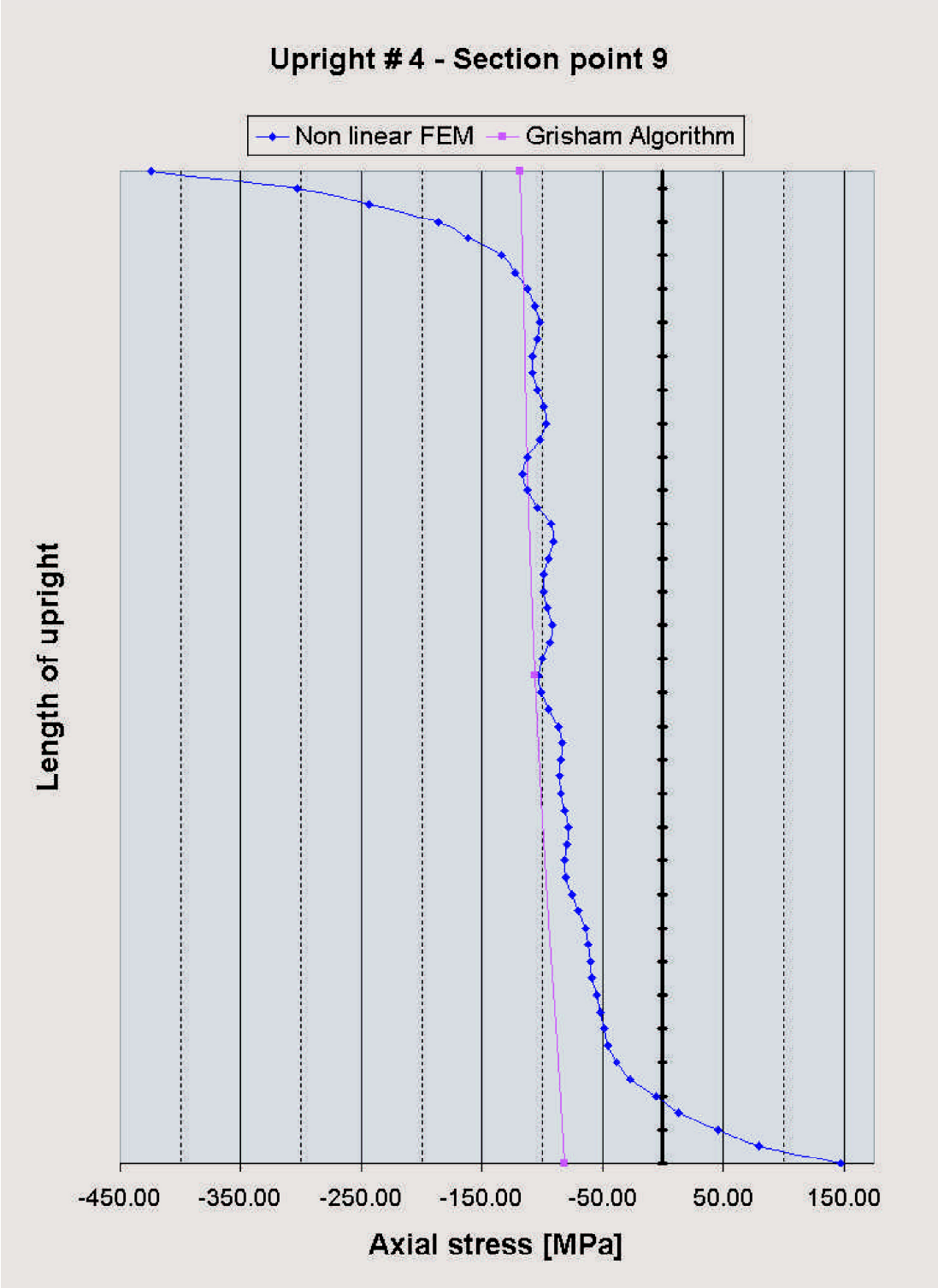

Figure 3.20: Comparative stress values in upright 4 at section point 9

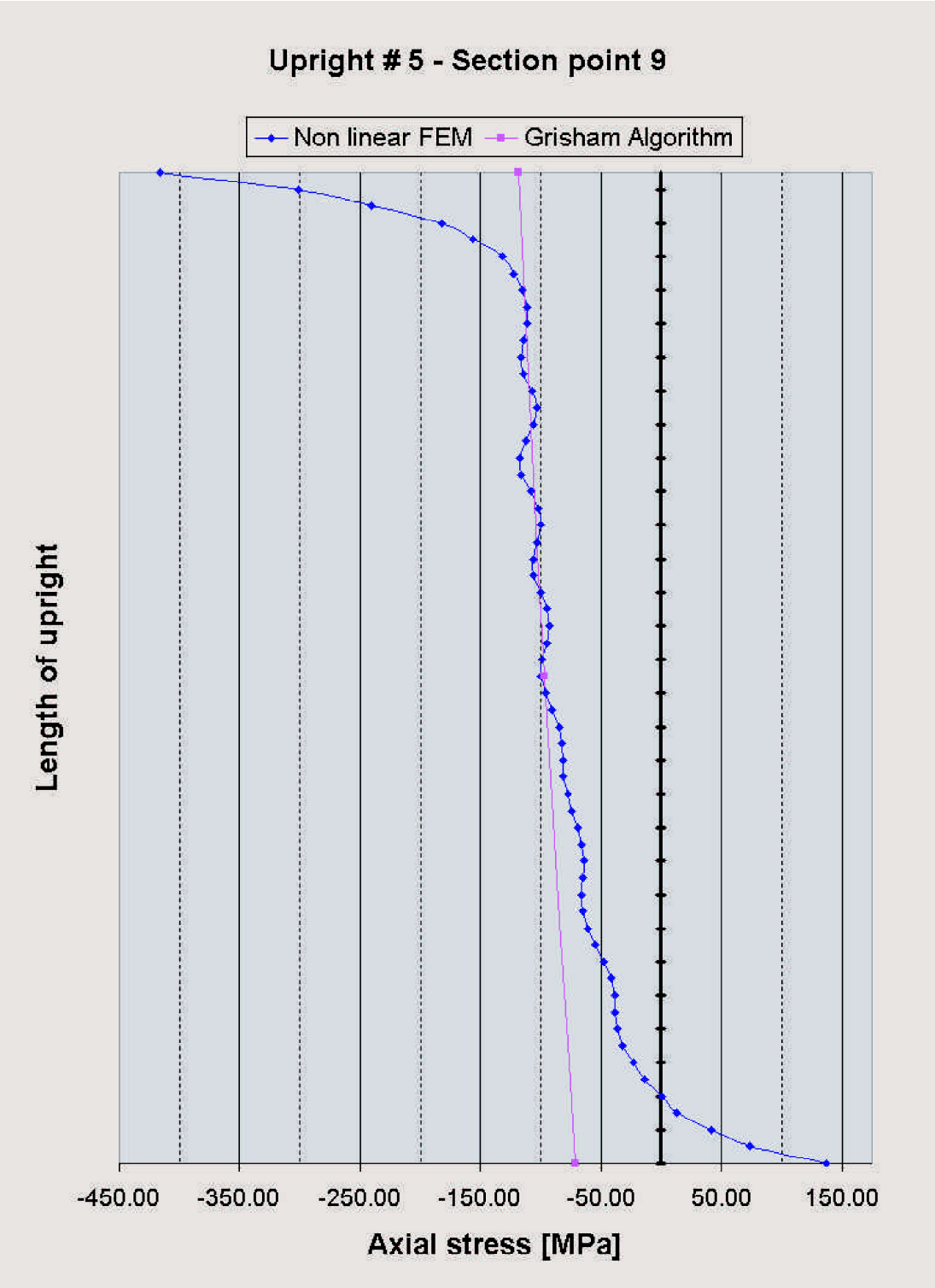

Figure 3.21: Comparative stress values in upright 5 at section point 9

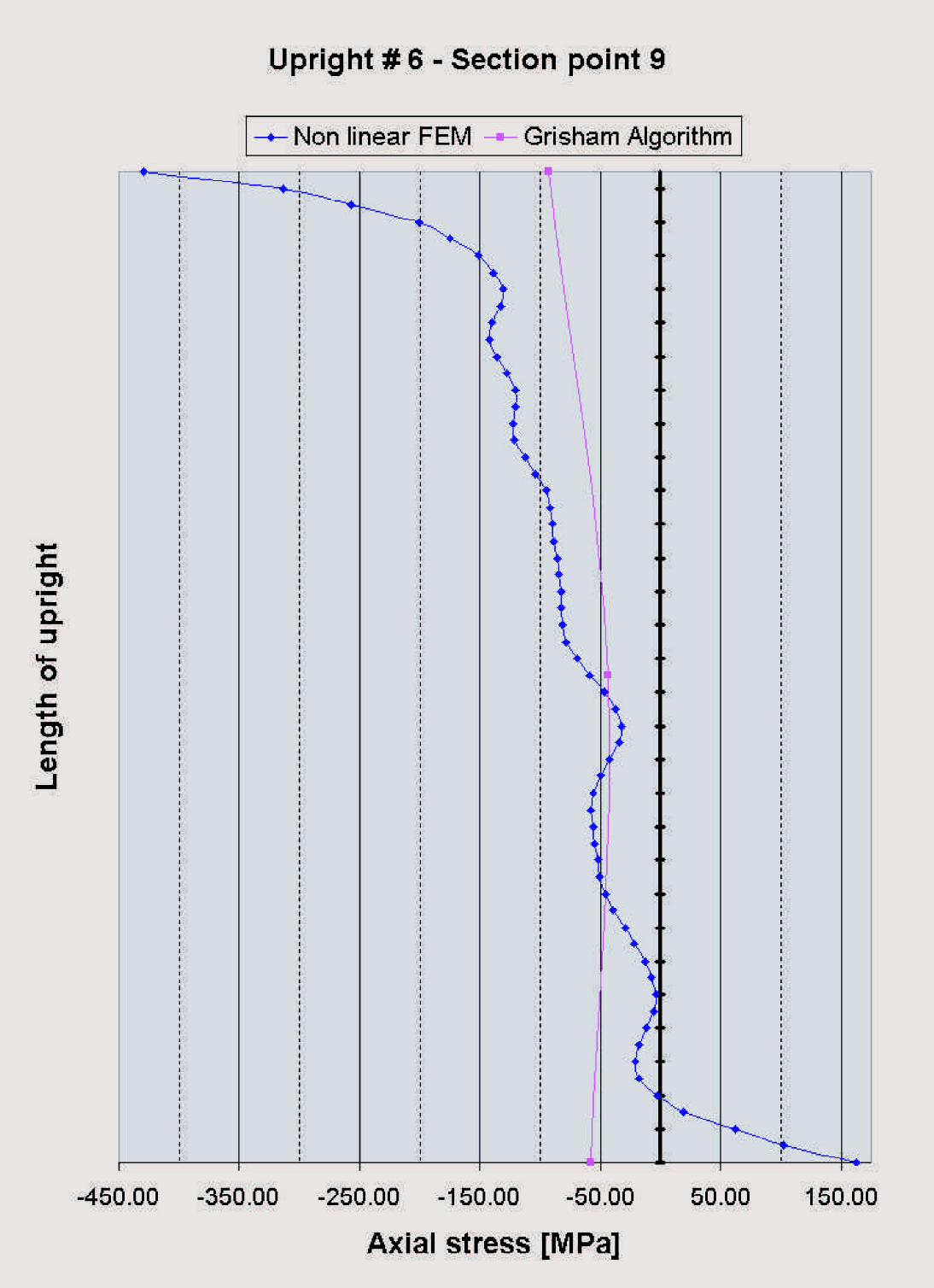

Figure 3.22: Comparative stress values in upright 6 at section point 9

3.5 Flange results

Table 3.2 shows the stress results in the upper and lower flanges of the non-linear finite element model compared to that of the Grisham algorithm. The correlation is reasonable, although it is noticed that the Grisham results are no longer conservative.

	Grisham Algorithm	Non-linear FEM
σ_{f_u} [MPa] (upper fibre)	-216.9	-259.4
σ_{f_u} [MPa] (lower fibre)	-255.0	-389.4
σ_{f_l} [MPa] (upper fibre)	162.9	196.7
σ_{f_l} [MPa] (lower fibre)	275.2	292.7

Table 3.2: Flange stress values at section A-A (Figure 2.1): non-linear finite element analysis

3.6 Deflection results

The displaced shape of the model, as viewed from the side, is shown in Figure 3.23. The out-of-plane displacement results of the analysis are shown in Figures 3.24 to 3.27. Figure 3.24 shows the onset of shear buckling after 13 load increments (at an applied shear load of 1552 N). Figures 3.25 and 3.26 show increased effects of shear buckling after 20 and 30 load increments into the analysis respectively. Figure 3.27 shows the final displaced shape after 102 load increments (at an applied shear load of 60 048 N).

Figure 3.28 shows a plot of the structure's displaced shape as viewed from a small angle off the mid-plane of the beam. This allows the "folds" in the webs, caused by diagonal tension effects, to be seen clearly. This is of course not visible in the linear finite element model in the Grisham algorithm. The maximum tensile principal stress in the sheet occurs parallel to these "folds" while the minimum principal stress occurs perpendicular to the "folds" and is usually in compression.

Figure 3.29 shows the displaced shape of the upper frame only (without the shell elements) so that the deformation of the upper flange and uprights can be viewed more clearly. The concave shape in the upper flange is due to the vertical components of the web stress (diagonal tension action pulling down), causing bending in the flanges between the uprights. The lower flange has a similarly displaced shape due to the diagonal tension effect.

The deflection of the structure is another variable that can be used for comparative and validation purposes between the non-linear finite element results and the Grisham algorithm results. The bottom node of the loaded end deflected 22.3 mm for the Grisham algorithm and 25.05 mm for the non-linear finite element model.

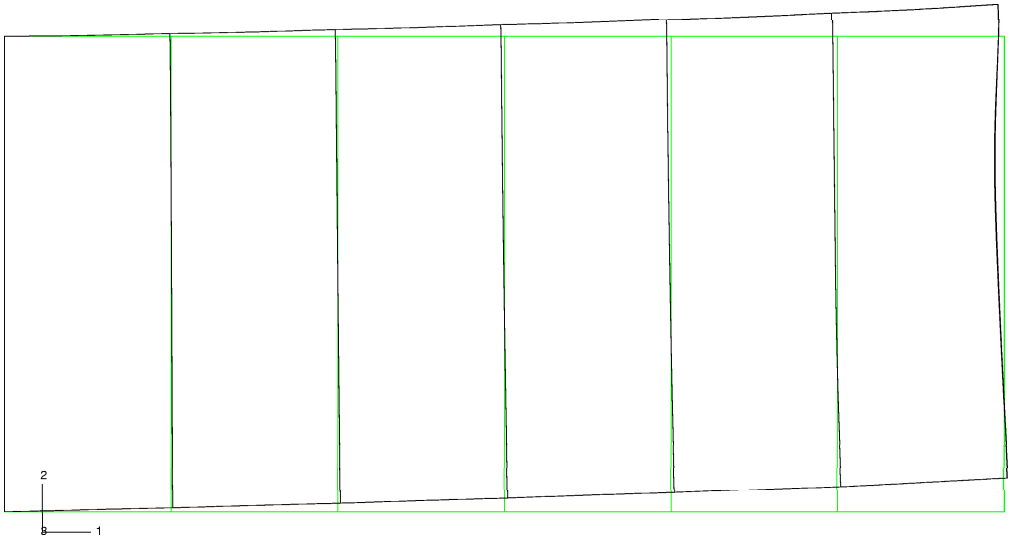

Figure 3.23: Displaced shape of beam viewed from the side

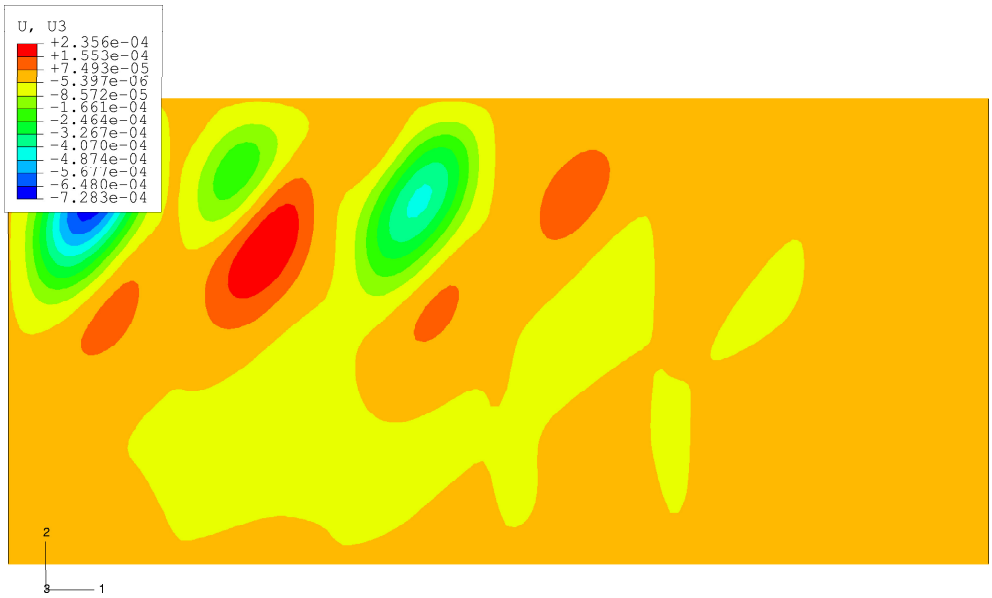

Figure 3.24: Onset of shear buckling - after 13 load increments (at an applied shear load of 1 552 N)

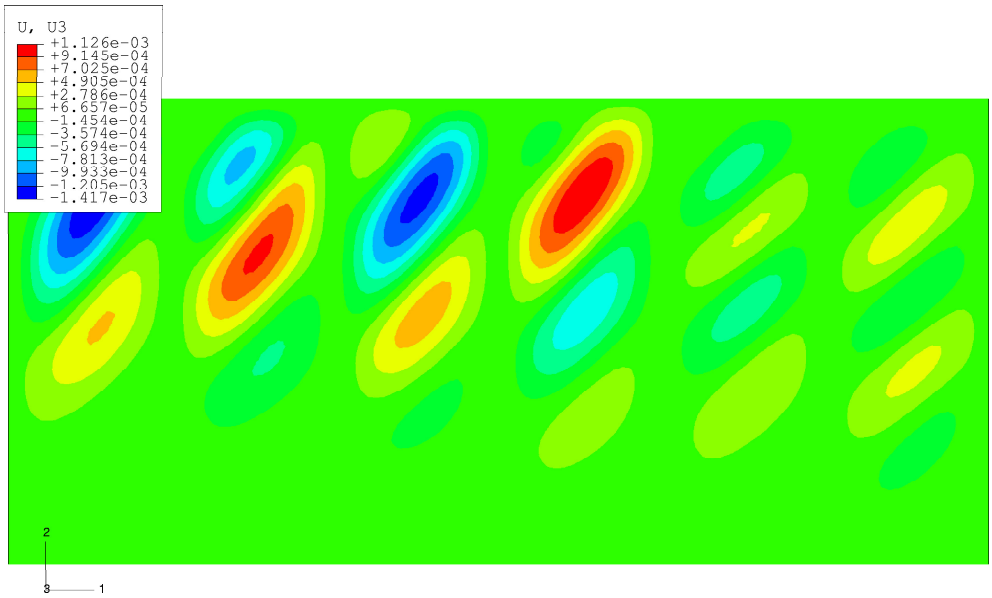

Figure 3.25: Progressive shear buckling - after 20 load increments

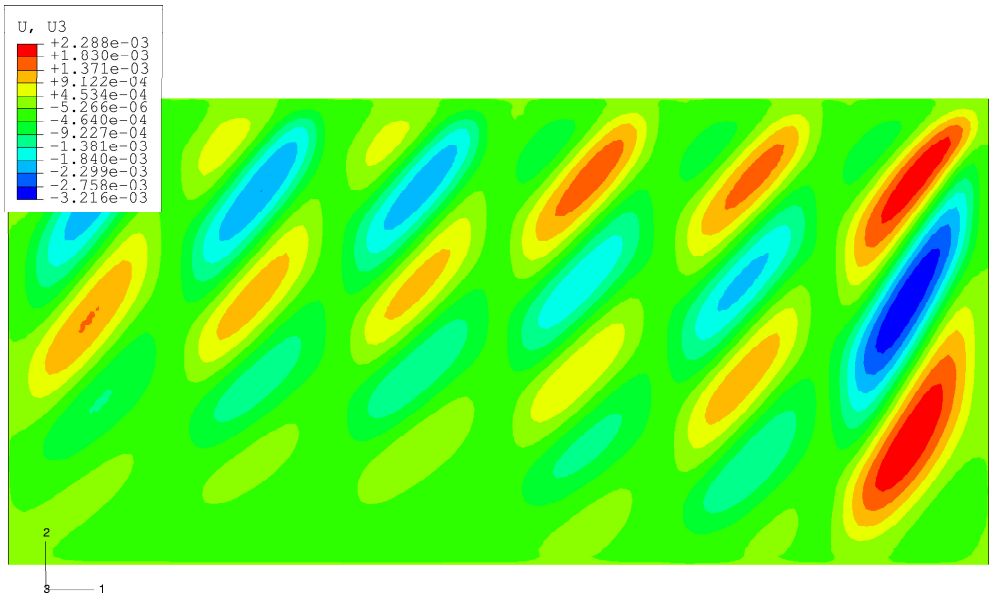

Figure 3.26: Severe shear buckling - after 30 load increments

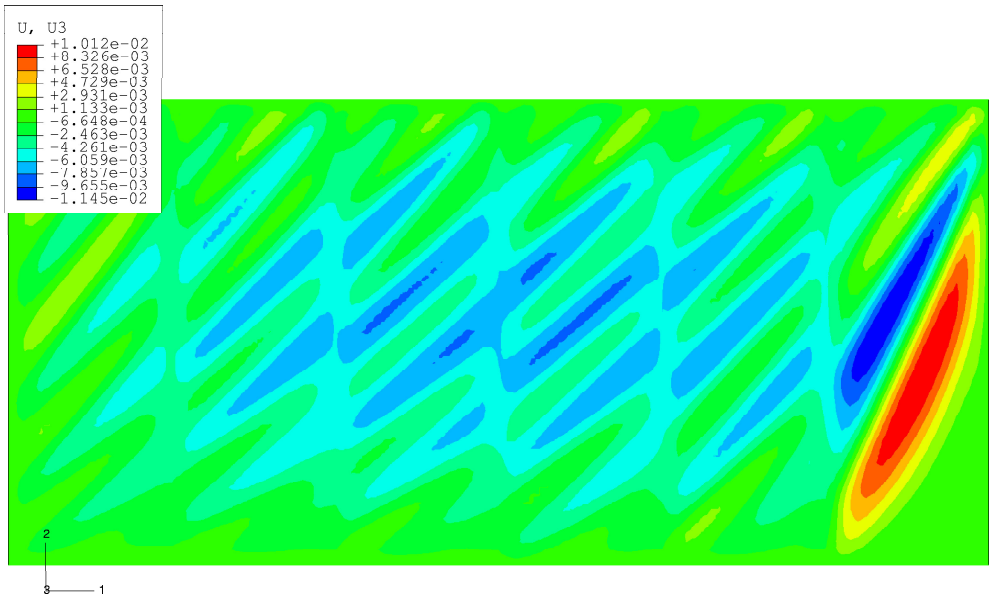

Figure 3.27: Excessive shear buckling at the end of the analysis - after 102 load increments (applied shear load of 60 048 N)

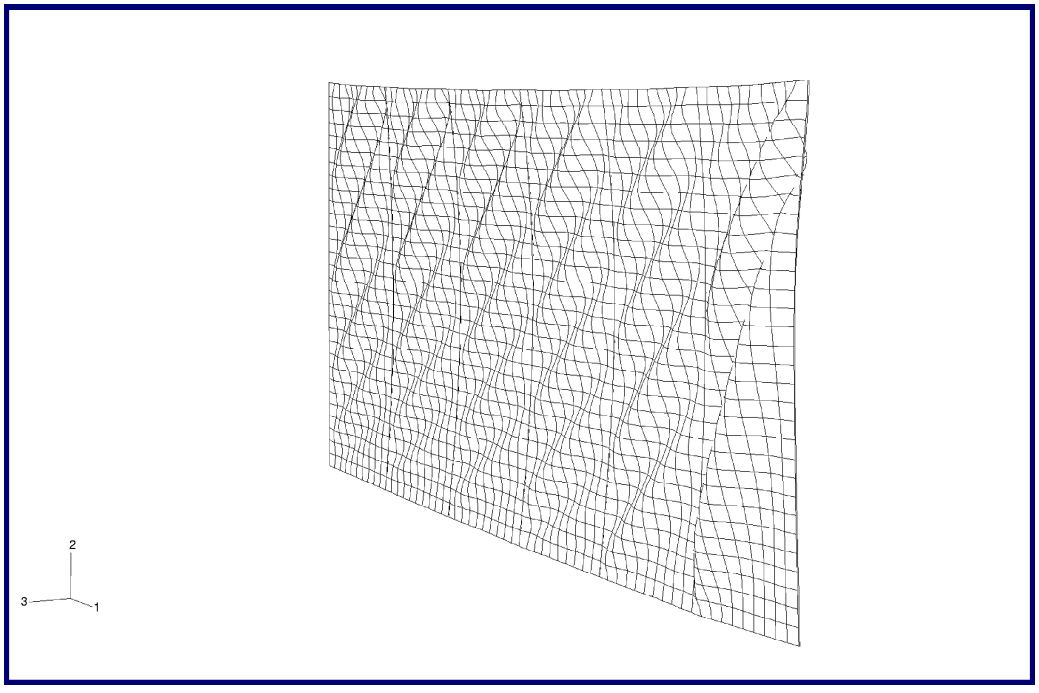

Figure 3.28: "Folds" visible in the displaced geometry

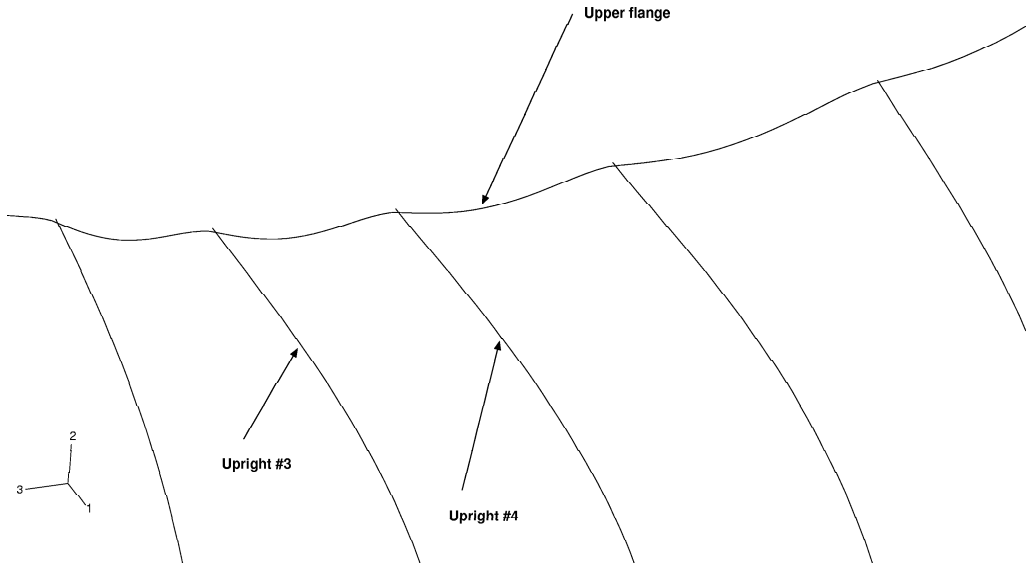

Figure 3.29: Upper flange deformation due to diagonal tension

3.7 The damping factor

For the example problem considered, the damping factor $c = 1.24 \times 10^6$ is the default value selected by the ABAQUS® finite element analysis software. The sensitivity of the factor at the onset of buckling of the structure is investigated in Table 3.3. The results show that the damping factor has a very small effect on the onset of buckling for lower values of c than the default value. Even values slightly higher have little effect and only once the damping factor is increased 1000 $\times$, is a significant effect noted. The value of the damping constant is therefore considered not to have a large influence on the results of the non-linear finite element analysis.

c	S_b
1.24×10^9	11828
1.24×10^7	1747
1.48×10^6	1552
1.24×10^6	1169
0.99×10^6	1163
1.24×10^5	1163
1.24×10^3	1163

Table 3.3: Damping factor c versus shear load at onset of buckling S_b

3.8 Mesh convergence study

A convergence study was done to ensure a reasonably inexpensive, yet adequately converged, finite element mesh. Table 3.4 shows that a discretization of 3×10 is sufficient. The discretizations in Table 3.4 are all selected to ensure acceptable element aspect ratios.

Mesh	τ_{cr}
1×3	2.446
3×10	2.315
5×15	2.314
10×30	2.356
20×60	2.380
30×90	2.388

Table 3.4: Mesh discretization versus critical buckling stress τ_{cr}

3.9 Run-time comparison

A run-time comparison between the Grisham algorithm and the non-linear finite element analysis is now used to indicate which method is more efficient from a computational point of view. In order to do this effectively, identical mesh discretizations are used for the two models. The results are shown in Table 3.5, where the mesh given represents the mesh for the web of *each* panel. All analyses were run on a HP C200 workstation. Although cpu times would be better, wall clock times are used in this comparison because the Grisham algorithm code can only log real time. Cpu times would give the effective time that the workstation spent on each run (process).

	Time	
Mesh	Grisham Algorithm	Non-linear FEM
3×3	31 secs	7 mins, 42 secs
10×30	30 min, 39 secs	4 hours, 59 mins

Table 3.5: Total wall-clock times for the Grisham method and non-linear finite element analysis as a function of mesh discretization

The Grisham algorithm is run with β-values which allow for the solution to converge (see Chapter 4). An initial estimate is made for the first run, after which minor adjustments are made until the solution converges. This is achieved within 2 to 3 iterations. The results indicate that the Grisham algorithm presents *an efficient and simple methodology for initial design sizing.*